Jurnal Teknologi

Full Paper

THERMAL INPUT EFFECTS ON THE MICROSTRUCTURE AND ELECTRICAL PERFORMANCE OF ZNO-CATIO$_3$ VARISTOR CERAMICS

Abdul Mu'iz Aniq Aiman Mohd Suhaimi[a], Malia Athirah Badruddin[a], Muhammad Syaizwadi Shaifudin[a], Wan Mohd Ikhmal Wan Mohamad Kamaruzzaman[a], Nur Aiman Syafiq Mohd Hamidi[a], Nursabrina Amirah Mohd Nasir[a], Nurul Ashraf Razali[b], Mohd Sabri Mohd Ghazali[a*]

[a]Faculty of Science and Marine Environment, Universiti Malaysia Terengganu, 21030, Kuala Nerus, Terengganu, Malaysia
[b]Faculty of Ocean Engineering Technology, Universiti Malaysia Terengganu, 21030, Kuala Nerus, Terengganu, Malaysia

Article history
Received
27 October 2024
Received in revised form
9 December 2025
Accepted
18 December 2025
Published Online
29 August 2026

*Corresponding author
mohdsabri@umt.edu.my

Graphical abstract

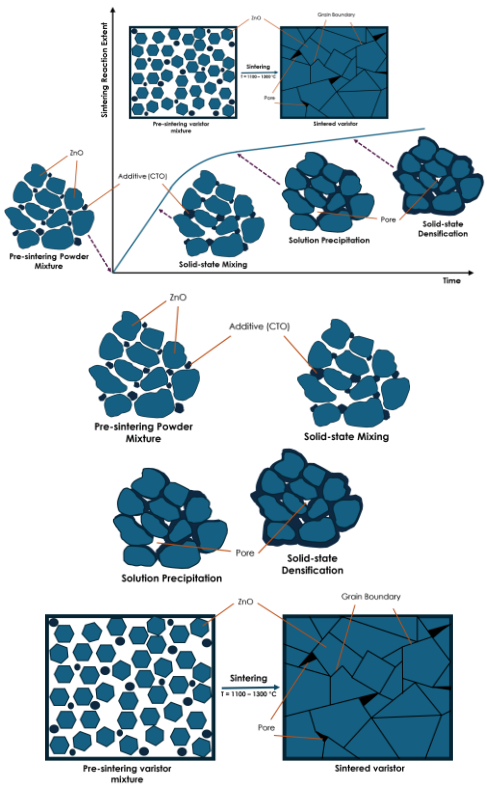

Abstract

Using a traditional solid-state mixed oxide method, pelletized polycrystalline zinc oxide-based varistor ceramics were prepared with calcium titanate ($CaTiO_3$) doping. This study examined how varying sintering temperatures affect the microstructural and electrical characteristics of the composite varistors. The samples were subjected to sintering temperatures between 1100 and 1300 °C for 90 minutes. X-ray diffraction (XRD) assessment confirmed the presence of two primary phases in the synthesized compound. Scanning electron microscopy (SEM) results showed that higher sintering temperatures promoted ZnO grain growth, increasing the average grain size from 4.66 to 10.42 µm. The average relative density of the synthesized samples exceeded 94% of the theoretical density. These results were determined to correspond with the modification in electrical properties, as the specimen sintered at 1250 °C demonstrated the most favorable electrical response, of which the nonlinear coefficient, breakdown voltage, and barrier height were 3.85, 0.99 V/mm, and 0.66 eV, respectively. The study presented in this paper can be used to discover and develop new and more efficient ZnO suppressors.

Keywords: Sintering, ZnO varistor, calcium titanate, microstructure, electrical properties

Abstrak

Menggunakan kaedah tradisional campuran oksida keadaan pepejal, seramik varistor berasaskan zink oksida polikristal yang dipelletkan telah disediakan dengan pendopan kalsium titanat ($CaTiO_3$). Kajian ini meneliti bagaimana variasi suhu pensinteran mempengaruhi ciri-ciri mikrostruktur dan elektrik varistor komposit. Sampel tersebut telah dikenakan suhu pensinteran antara 1100 hingga 1300 °C selama 90 minit. Penilaian pembelauan sinar-X (XRD) mengesahkan kehadiran dua fasa utama dalam sebatian yang disintesis. Hasil mikroskopi elektron imbasan (SEM) menunjukkan bahawa suhu pensinteran yang lebih tinggi mempromosikan

pertumbuhan butiran ZnO, meningkatkan saiz purata butiran dari 4.66 hingga 10.42 µm. Purata ketumpatan relatif sampel yang disintesis melebihi 94% daripada ketumpatan teori. Keputusan ini didapati sepadan dengan pengubahsuaian dalam sifat elektrik, di mana spesimen yang disinter pada suhu 1250 °C menunjukkan tindak balas elektrik yang paling baik, dengan pekali tak linear, voltan pecah, dan ketinggian halangan masing-masing adalah 3.85, 0.99 V/mm, dan 0.66 eV. Kajian yang dibentangkan dalam kertas ini boleh digunakan untuk meneroka dan membangunkan alat penyekat ZnO yang baharu dan lebih cekap.

Kata kunci: Suhu pensiteran, ZnO varistor, kalsium titanat, mikrostruktur, sifat elektrik

1.0 INTRODUCTION

Electrical devices are invented to endure specific voltages. If exposed to voltages beyond their design limits, damage may occur. Even small voltage surges could cause damage over time because the longer they are experienced, the greater the damage will likely be. Surge and transient protection are thus required to ensure the reliable operation of machinery and devices vulnerable to abnormal overvoltage [1, 2]. It is prudent to use surge protection to mitigate the risks of voltage surges. In the modern surge protection industry, metal oxide varistors (MOVs), primarily referred to as zinc oxide (ZnO) varistors, are currently the best surge devices available for overvoltage arresters when subjected to overload transients due to their ability to sense and handle large amounts of passing energy for their physical and worth [3-5].

ZnO has lately evolved as a versatile semiconducting metal oxide material owing to its good performance in surge energy absorption, sensing, high optical transparency [6], tuneable electronic properties, ease of synthesis, low cost, and low toxicity [7-9]. ZnO-based varistor contains a mass of sintered n-type ZnO particles embedded in a mixture of different metal oxides such as Bi_2O_3, Pr_6O_{11}, Co_3O_4, MnO, Sb_2O_3, TiO_2, and Cr_2O_3 [10-12]. Varistor ceramics are traditionally manufactured using the solid-state ceramic fabrication method of sintering temperature typically at 1100 to 1300°C with 1 to 3 h soaking time [7, 13]. During sintering, ZnO interacts with dopants, creating a thin insulating layer that forms Double Schottky Barriers (DSBs) at the grain boundaries. This interaction results in nonlinear current-voltage behavior [14, 15]. The behavior of ZnO varistors in terms of their electrical characteristics is significantly impacted by the erratic movement of defects within the material. This unpredictable defect migration leads to variations in the size of the grains, the boundaries between these grains, and the regions where charge carriers are depleted. The formation of DSBs is fundamentally driven by the migration of point defects, notably oxygen vacancies and zinc interstitials. The potential barriers height that causes the nonlinear switching trait is developed when these defects build up at the grain interfaces. However, unpredictable defect migration can trigger inhomogeneity in barrier height and the emergence of leakage pathways which eventually limiting device functionality [16].

Beyond the influence of various additives, the sintering or firing process of ceramic materials plays a crucial role in determining the intricacies of the interfaces and the overall microstructure. This process also significantly affects the electrical and dielectric properties of ZnO varistors [17]. Even though the control of critical parameters such as grain size, additive uniformity, and selective dopants have been studied for decades, it is required to consider the optimization of the sintering temperatures and processes for developing efficient ZnO varistor materials. Subjecting the varistor powder particles to high temperatures in the firing process supplies the energy needed for binding during compaction stages, leading to the rapid growth of grains [18]. In addition, the pores that exist in the microstructure will shrink because of the sintering temperature and time [19]. However, the advanced heat treatment modifications to regulate grain growth were quite expensive and energy-consuming to be fully implemented.

The growing interest in micromachining has resulted in an increased production of varistors for low-voltage applications. The addition of additives featuring a large ionic radius is observed to improve the nonlinearity of the varistor with low breakdown voltage [20]. The incorporation of perovskite structure, calcium titanate ($CaTiO_3$) as a varistor former seems to have a better effect on microstructure and enlargement of the ZnO grains since it contains TiO_2, a solid grain growth enhancer [21]. The presence of TiO_2 within additive aids in densification process by minimizing porosity and fostering the development of large ZnO grains which a critical physical feature for optimizing varistors for low voltage use [22]. Furthermore, the ionic radius of Ca^{2+} (0.99 Å) is greater than Zn^{2+} (0.74 Å), causing structural deformities in the crystal structure and affecting its electrical behaviors [23]. Upon incorporation into the ZnO crystal lattice, this disparity induces structural deformation and lattice stress.

Such structural perturbations directly affect the defect states at grain boundaries, which in turn modifies the potential barrier properties and the resulting nonlinear electrical behavior of the varistor [24]. Extensive studies on the influence of $CaTiO_3$ on the structural characteristics and electrical performance of ZnO varistors have been limited so far. To better comprehend the performance of ZnO varistors under specific conditions, researchers have concentrated on investigating the effect of sintering temperature on grain growth, using a cost-effective additive.

2.0 METHODOLOGY

2.1 Sample Preparation

ZnO-$CaTiO_3$-based varistors were fabricated by the traditional solid-state mixed oxide method, as shown in Figure 1. Analytical grade ZnO powder (99.99%, Aldrich) and $CaTiO_3$ powder (99%, Aldrich) were weighed as the pioneer oxide materials in this study with the molar composition of 99.0 mol% ZnO + 1.0 mol% $CaTiO_3$. The dopant concentration was maintained at 1.0 mol% throughout the study to serve as a controlled parameter, allowing for systematic evaluation of sintering temperature effects (1100–1300 °C) on the varistor properties. The powders underwent thorough processing within a planetary ball mill for a duration of 120 mins using stainless steel balls with the required set-up. 1.75 wt.% of binding agent, polyvinyl alcohol (PVA), was mixed into the milled powder to offer good strength to the pressed pellets. After drying at 90°C, the mixture was crushed with a porcelain agate mortar and sifted through a 75 µm sieve to obtain a fine powder. The samples were dried at 90 °C to remove moisture without degrading the PVA binder or inducing cracking in the green pellets. Next, a small amount of subsequent sieved powders was fortified into homogeneous pellets of 10 mm diameter at 2.6 T/min with a thickness of 2 mm. The pellets were subsequently held for 90 minutes at varying sintering temperatures of 1100 °C, 1150 °C, 1200 °C, 1250 °C, and 1300 °C, with a regulated heating and cooling rate of 3 °C per minute, as illustrated in Figure 2. To form silver electrodes, selected pellets from each sintering temperature were coated on both surfaces with conductive silver paste, resulting in electrodes that are 6 mm in diameter.

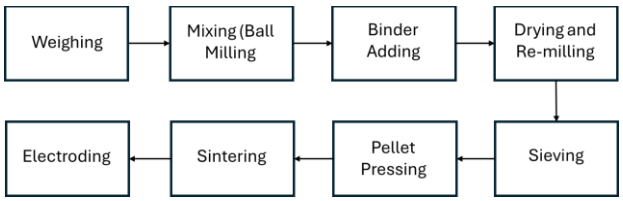

Figure 1 The simplified flow diagram of the steps involved in the varistor fabrication process

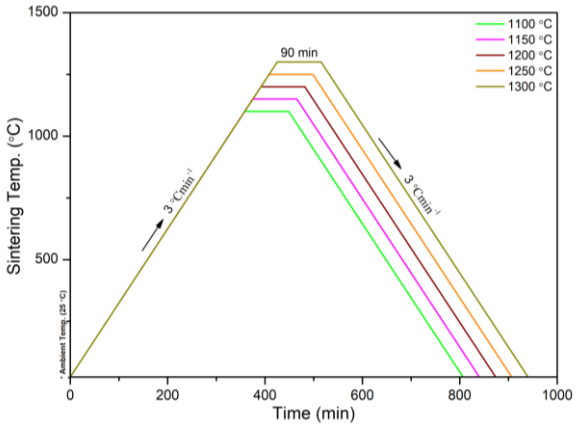

Figure 2 ZnO varistor samples of various sintering processes

2.2 Sample Appraisal

The crystalline phases and lattice planes were identified using a Rigaku MiniFlex II XRD with CuKa emission supply. The scanning of 2θ angles is from 20° to 80°. The physical surface structure of sintered pellets was examined under the SEM (Tescan Vega) connected with energy dispersive X-ray (EDX) spectroscopy. The analysis aims to determine co-existing elements and quantify their distribution on grains and grain boundaries. The average grain size, *d*, of ZnO grains in the varistor ceramic was predicted by measuring the grain size from SEM micrographs, with the employment of the lineal intercept method introduced by [25], as follows:

$$d = 1.56L/MN \quad (1)$$

where *L* denotes the random line length on the micrograph, *M* signifies the magnification of the image, and *N* indicates the number of grain boundaries intersected by the lines. The factor 1.56 serves as the correction element required to convert an average intercept width into an average grain size [26]. The experimental density of the sintered pellets was measured by operating electronic densimeter at standard temperature using the Archimedes principle with distilled water as the immersion medium. The electrical behaviors of sintered pellets were measured using a Keithley 2410-(SCS) semiconductor characterization system. The electrical coefficient of nonlinearity, *α* of the ZnO-based varistor was calculated according to the current density-electric field, *J-E* properties at room temperature. The breakdown voltage, E_b, was determined from the *J-E* curve at a current of 1.0 mA, while the leakage current density, J_L, was measured at 0.80 E_b, and the interface barrier height, Φ_B, was also calculated.

3.0 RESULTS AND DISCUSSION

3.1 Scanning Electron Microscopy (SEM) with Energy Dispersive X-ray (EDX) Analysis

Figure 3 represents the physical surface structure of sintered samples. It has been found that the structure of each sample consists of two types of grains: large grains as prime phases due to their large quantity and appearance as ZnO grains on the microstructure and small intergranular grains as secondary phases. Based on Figure 3, the formation of compact grains and grain boundaries were clearly observed. Despite the economic attraction of the solid-state approach, a significant drawback of the method is the challenge of acquiring a fine and compositionally uniform microstructure [27]. An important alteration in the dimensions of the grains was noted as the sintering temperature increased, suggesting that the sintering temperature plays a crucial role in governing the growth of the grains. Table 1 provides a comprehensive overview of all pertinent data, whereas Figure 4 illustrates the variations in both average grain size and relative density in relation to different sintering temperatures.

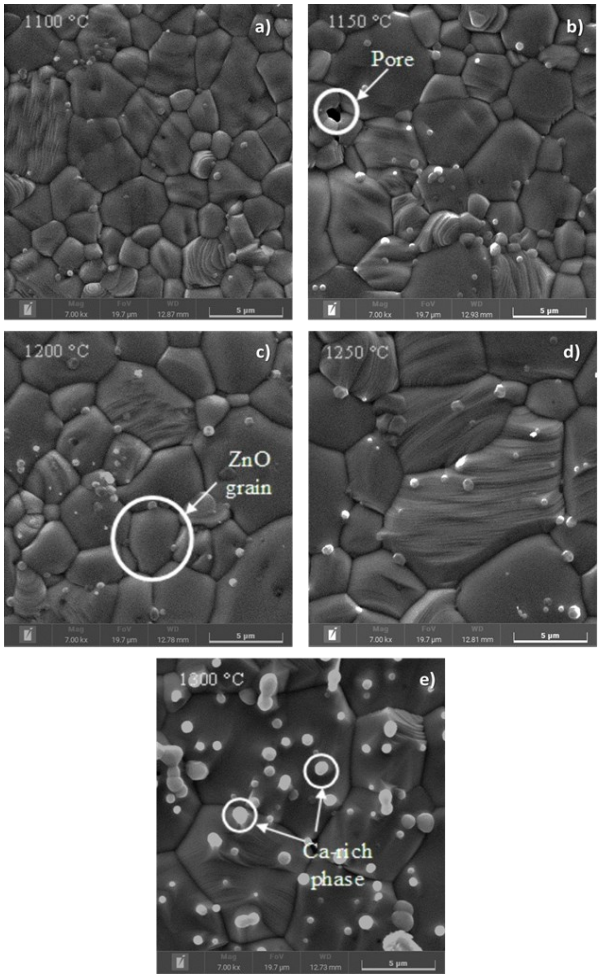

Figure 3 SEM micrographs (7 kx magnification) of ZnO-$CaTiO_3$ based varistor sintered at a) 1100 °C, b) 1150 °C, c) 1200 °C, d) 1250 °C, and e) 1300 °C

Table 1 Average grain size and relative density of ZnO-$CaTiO_3$ varistor ceramics subjected to various sintering temperatures

Thermal Input (°C)	Average grain size, d (µm)	Theoretical density, ρ_{th} (g/cm³)	Experimental density, ρ_{ex} (g/cm³)	Relative density, ρ_{rel} (%)
1100	4.66	5.648	5.581	98.81
1150	6.18	5.648	5.323	94.25
1200	7.50	5.648	5.457	96.62
1250	8.84	5.648	5.462	96.71
1300	10.42	5.648	5.465	96.76

According to Wong [28], ZnO grain growth typically increases with higher sintering temperature and duration. As the temperature for sintering increased from 1100 °C to 1300 °C, the mean grain dimensions expanded progressively to 4.66 µm, 6.18 µm, 7.50 µm, 8.84 µm, and ultimately 10.42 µm. Observations from Figure 3 show that the specimen sintered at 1150 °C contained several pores, along with some grains that were disproportionately large. The relative density assessment indicated that these pores contributed to a reduction in the material's density, which in turn caused leakage currents. In comparison, when the sintering temperature was elevated to 1300°C, the quantity of pores diminished, resulting in the relative density of all specimens exceeding 94%. This is due to the removal of voids during grain growth, and TiO_2 assisted grain growth as a significant grain enhancer, making it a decisive additive for promoting crystal growth to fabricate low-voltage ceramics [29]. Furthermore, high thermal conditions supply a prominent propulsion force for the internal atomic diffusion that is necessary for grain growth and pore removal [30].

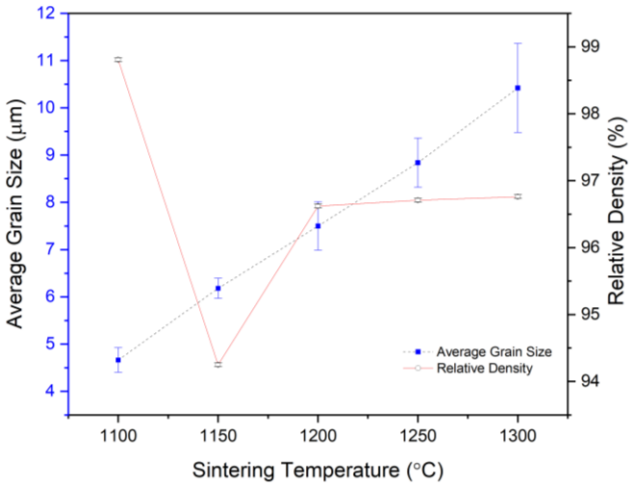

Figure 4 Average grain size and relative density of sintered samples

As thermal levels rise, the sintered samples displayed wavering behaviour on the relative density ranging from 94.24% to 98.81% due to the holes emergence that evidently identified by SEM

micrograph in Figure 3. The oxygen outflow from the ZnO structure, emanating from the oxygen vacancy during densification reaction resulted in the unification consequence of porosity [31]. With continued rises in heat application, less than 3.5% of porosity for ceramics sintered above 1200 °C were observed, which later improved the density of the varistor ceramics.

Table 2 EDX results of ZnO varistor composite with different sintering temperatures

Sintering temperature (°C)	Energy of X-ray emitted by elements (keV)			
	Zn	O	Ca	Ti
1100	83.13	16.05	0.28	0.54
1150	82.89	15.95	0.49	0.67
1200	83.18	15.80	0.56	0.46
1250	81.88	15.64	1.12	1.36
1300	79.34	16.19	2.17	2.30

The dispersion and existence of elements on the ZnO-$CaTiO_3$ composite varistor ceramic were displayed by the EDX mapping, as shown in Figure 5.

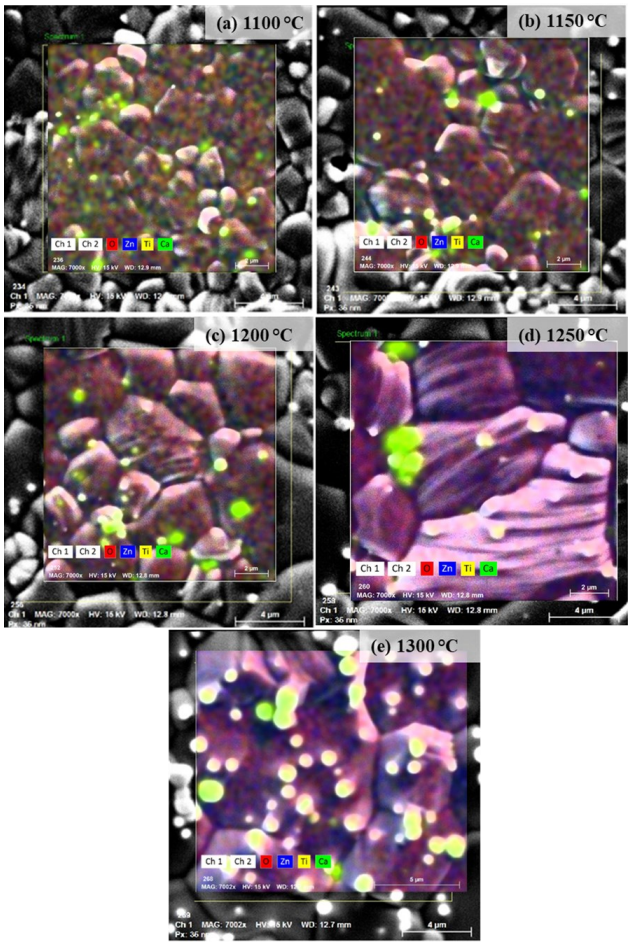

Figure 5 Elemental dispersion of ZnO-$CaTiO_3$ varistor ceramics at different sintering temperatures: (a) 1100 °C, (b) 1150 °C, (c) 1200 °C, (d) 1250 °C, and (e) 1300 °C

Different colors represent various energy of the elements, where red, blue, yellow, and green depicted the presence of oxygen, zinc, titanium, and calcium, respectively. Zn (blue) has a uniform distribution on the whole sample, but there is no overlapping of energy between Zn, Ca, and Ti in certain regions. The EDX results in Table 2 reveals the reduction of oxygen (red-coloured energy) content in the sintered ceramics at thermal input up to 1250 °C, which imputed the oxygen-element reactions amid thermal processing. Moreover, this interplay apparently shown the structuring of broader ZnO grains during heat treatment is because of the oxygen embedding into Zn matrix. The presence of $CaTiO_3$ is obvious at the grain border in Figure 5 (d), where this can be an optimal choice for the intergranular region in ZnO ceramics because its oxygen content enhances the voltage-clamping capability [32].

3.2 X-ray Diffraction (XRD) Analysis

The crystal structure of ZnO-$CaTiO_3$ varistors, synthesized at sintering temperatures ranging from 1100 °C to 1300 °C, was analyzed using X-ray diffraction (XRD) spectroscopy. Figure 6 demonstrates the notable variations in the diffraction patterns across different samples, emphasizing their individual diffraction spectra. With $CaTiO_3$ consistently held at a 1.0 mol% concentration, the sintering duration was fixed at 90 minutes to investigate how sintering temperature influences both the microstructure and electrical nonlinearity. The XRD examination displayed that the predominant phase of ZnO materials and a small amount of $CaTiO_3$ were found in the various samples. The diamond (♦), the heart (♥), and the clover (♣) symbols represent the Bragg position of the ZnO (JCPDS card no. 01-080-3004), $CaTiO_3$ (JCPDS card no. 01-078-5896) and Zn_2TiO_4 (JCPDS card no. 01-087-9921) phases in the sintered ZnO samples, respectively.

All sintering conditions exhibited the phases of $CaTiO_3$; meanwhile, spinel phases Zn_2TiO_4 were only displayed for the samples sintered at 1100-1200 °C. The ratio of the spinel phase to the ZnO primary phase is relatively small, as seen by the weak peak intensities. The results indicate that the use of high sintering temperatures contributes to the reduction of Zn_2TiO_4 phases. Specifically, firing ZnO-CTO ceramics at temperatures exceeding 1200 °C effectively prevents the formation of the spinel phase. The Zn_2TiO_4 spinel phase, which typically forms at intermediate temperatures (600 to 1000°C) [33], exhibits thermal instability above 1200 °C. At these elevated sintering temperatures, the spinel either dissolves into the ZnO matrix or decomposes, with reaction kinetics favoring the formation of ZnO-based solid solutions over secondary phase retention. This phenomenon accounts for the absence of Zn_2TiO_4 in samples sintered at 1200 °C and above, where TiO_2 primarily acts as a grain growth modifier rather than

forming a distinct spinel compound [34]. This spinel phase can be observed due to the interaction of titanium dioxide and zinc oxide, resulting in partial substitution of Ti^{4+} with Zn^{2+}. Due to the presence of excess ZnO in a solid solution, Zn^{2+} can readily incorporate into TiO_2 and form Zn_2TiO_4. Zn^{2+} occupies the octahedral sites of TiO_2, while Ti^{4+} cannot occupy the tetrahedral sites of ZnO [35]. The highest peak is usually observed at the (101) plane of the ZnO phase, while the CTO phase appears at the (112) plane.

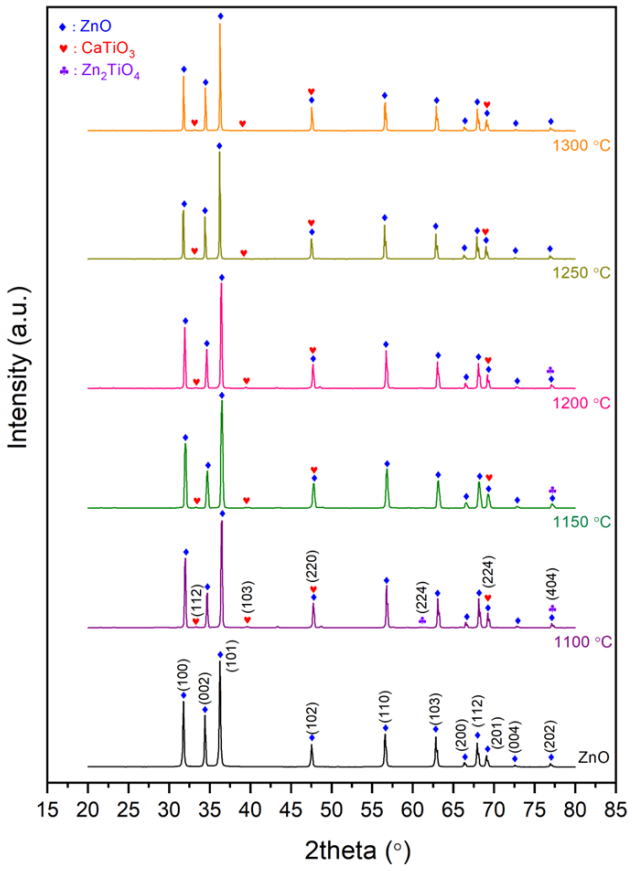

Figure 6 The XRD spectrum of ZnO-$CaTiO_3$ varistors with different sintering temperatures

Table 3 documents the variations in peak intensity for both the (101) and (112) planes, correlating the changes in angles with the peak strengths resulting from different thermal conditions.

Table 3 The Bragg angle and intensity shift of (101) and (112) planes with respect to sintering temperature

Temperature (°C)	Bragg Angle (°)		Intensity (a.u.)	
	ZnO (101)	$CaTiO_3$ (112)	ZnO (101)	$CaTiO_3$ (112)
RT	36.26	33.08	175177.78	27446.49
1100	36.50	33.26	100592.22	1026.67
1150	36.50	33.29	83697.48	641.27
1200	36.44	33.21	115970.55	930.68
1250	36.21	33.05	176790.70	1316.64
1300	36.26	33.08	104577.78	1998.89

The intensity of the ZnO peak at (101) plane is higher than the starting ZnO powder for specimens sintered at 1250°C and 1300°C, suggesting that the distribution of crystal structure is more uniform and fine in grain size compared to other sintered samples, as indicated by sharp and narrow peak intensity [36]. From the previous studies, the spinel phase, Zn_2TiO_4 is formed due to the decomposition of $ZnTiO_3$ at the firing temperature above 900 °C [37, 38].

A slight shift in the XRD patterns is illustrated in Figure 7, where the peaks of the (110) ZnO planes shift to the right in the 2θ direction for samples sintered at temperatures between 1100 and 1200 °C. This supports the observed decrease in peak strength in the XRD patterns for the specified ceramics, attributed to a decline in crystal quality that results in reduced crystallite size and d-spacing values. Additionally, the peaks for these three samples exhibit a broader full width at half maximum (FWHM), indicating imperfections or disorders within the crystal lattice. These defects, such as pores, were confirmed by the SEM images [39]. Table 4 provides the information of crystallite size (*D*), full width at half maximum (*FWHM*), and micro-strain (***ε***) for each of the sintered samples. Scherrer's equation was employed to determine the crystallite sizes from the peak broadening of the ZnO (101) plane in the XRD traces. The notable changes in the interaction between FWHM and crystallite size can best be described as the crystallite size increasing when the FWHM decreases. The peak broadening signifies the smaller crystallite size as well as higher micro-strain and hybrid composition in materials [40].

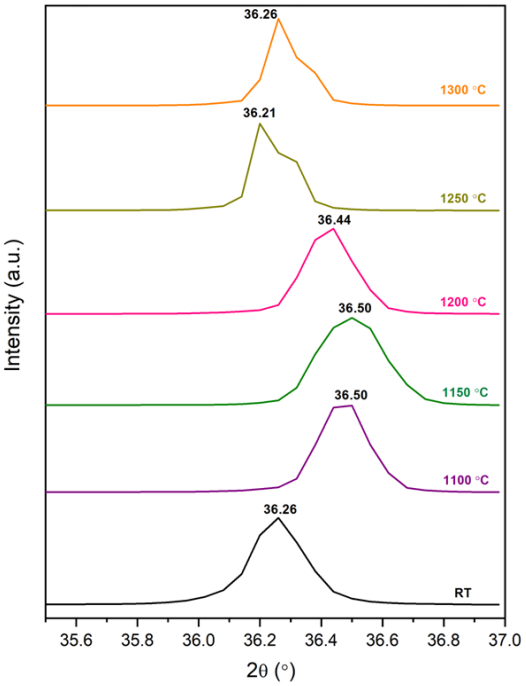

Figure 7 Expanded XRD peaks in the 35–37° of 2θ region.

Table 4 Structural features of ZnO-$CaTiO_3$-based varistors prepared at various sintering temperatures between 1100 °C and 1300 °C.

Sintering Temperature (°C)	FWHM, β (°)	Crystallite size, D (nm)	Micro-strain, ε (10^{-3})	d-spacing (Å)	Relative variation (%)
1100	0.187	44.72	2.48	2.58900	-0.567
1150	0.243	34.46	3.21	2.58900	-0.567
1200	0.189	44.34	2.50	2.59268	-0.426
1250	0.159	52.58	2.12	2.60688	0.120
1300	0.139	60.15	1.85	2.60376	0.000

The specimens sintered at 1150 °C appear to possess a broader ZnO (101) plane peak than others, as shown in Figure 7. Among all sintered samples, the specimen prepared at 1150 °C displayed the maximum micro-strain and minimum crystallite size (34.46 nm). Microstructural characterization by SEM confirmed the presence of substantial defects, including inhomogeneous phase distribution and pronounced porosity. These microstructural irregularities serve as scattering centers that disrupt coherent X-ray diffraction, leading to the maximum *FWHM* value documented in the investigation. The presence of defects (inhomogeneous composition and pore formation) in the microstructure, as depicted in Figure 3, might have contributed to the peak broadening for samples sintered at 1150 °C [30]. Oxygen vacancies represent intrinsic crystal imperfections in the ZnO structure. The oxygen deficiency creates lattice strain and reduces crystallite size, both of which lead to peak broadening in XRD patterns. This phenomenon is explained by the Scherrer equation, which establishes the inverse relationship between crystallite size and diffraction peak width [41]. No precise trend is observed in the relationship between sintering temperature and peak broadening, except for a notable increment in firing temperature from 1150 °C to 1300 °C. The increment leads to an increase in crystallite size, which results in the formation of narrower peaks in XRD traces.

3.3 Current Density-Electric Field (J-E) Characteristic Evaluation

The electrical traits of varistors, especially those resulting from sintering, best illustrate their properties. The current density-electric field (*J-E*) curve is used to characterize the electrical properties of selected sintered pellets, and the resulting data are shown in Figure 8. The feature curves of the various sintered samples can be roughly split into two areas: a linear area prior to the breakdown field and a nonlinear area subsequent the breakdown field. Alternatively, a better nonohmic feature is produced by the sharper knees of the curves between the two regions [30]. From Figure 8, the electrical parameters of ZnO-$CaTiO_3$ varistors were derived, including leakage current, breakdown voltage, and the nonlinearity coefficient at various sintering temperatures with a current density of 1.0 mA/cm². The nonlinearity coefficient, α, is calculated as the inverse of the slope of the *J-E* curves to determine how rapidly the material transitions from a high-resistance to a low-resistance state by absorbing potentially harmful surges [42]. Besides, the larger the nonlinear coefficient, the sharper the knee in the curves connecting the pre-breakdown and breakdown areas [43, 44]. The breakdown voltage is inversely related to grain size. Higher sintering temperatures promote grain growth, thereby reducing the number of grain boundaries per unit thickness. Since each boundary provides a discrete voltage barrier, fewer boundaries result in lower breakdown voltage values. Pores present in the ceramic matrix function as structural defects that interrupt electrical conduction pathways and reduce the available cross-sectional area for current transport. Samples exhibiting high porosity, such as those sintered at 1150 °C, demonstrate reduced relative density and correspondingly elevated leakage current density [45].

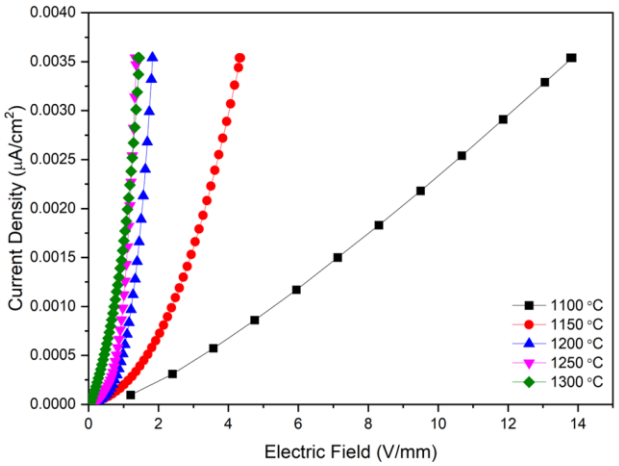

Figure 8 The *J-E* characteristic curves of ZnO-$CaTiO_3$ varistor with different sintering temperatures

The nonohmic electrical parameters of all sintered samples are summarized in Table 5. Elevation of the sintering temperature enhanced the nonlinear coefficient up until 1250 °C. Subsequent escalation in sintering temperature results in the intense drop of the nonlinear coefficient value. Table 5 reveals that the peak nonlinearity coefficient of 3.85 was obtained with specimens sintered at 1250 °C. Interestingly, there was a significant reduction in the breakdown voltage, which fell sharply from 5.32 V/mm to 0.75 V/mm as the sintering temperature rose. Hembram *et al*. (2020) suggest that a smaller ZnO grain size

correlates with a higher breakdown field [46]. However, this study contradicts their findings by demonstrating that the breakdown voltage diminished due to an increase in both ZnO grain size, and the sintering temperature. These results are corroborated by the SEM grain size analysis, which shows similar trends. Akinnifesi [44] found that the breakdown voltage decreases with increasing sintering temperatures because of the development and resultant growth of secondary phases at various temperatures.

Table 5 The electrical parameters of the ZnO-$CaTiO_3$ varistors sintered at various temperatures

Sintering Temperature (°C)	α	E_B (V/mm)	J_L (μA/cm²)	Φ_B (eV)	V_{gb} (V)
1100	1.32 ± 0.000	5.32	745.74	0.598	0.0244
1150	2.11 ± 0.012	2.39	647.19	0.633	0.0130
1200	3.17 ± 0.011	1.23	499.16	0.663	0.0109
1250	3.88 ± 0.020	0.99	425.11	0.666	0.0076
1300	1.90 ± 0.004	0.75	653.37	0.633	0.0078

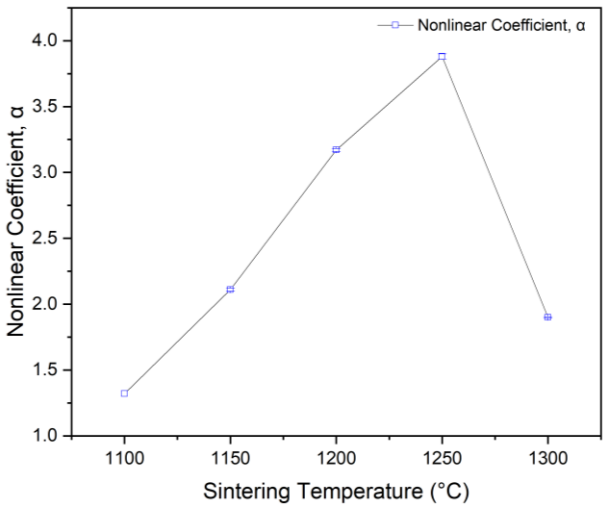

Figure 9 Nonlinear coefficient (α) of ZnO-$CaTiO_3$ varistors prepared at different sintering temperatures

Increasing the sintering temperature of the varistor material significantly improved the *α* value, reaching its peak at 1250 °C. However, any further rise in sintering temperature resulted in *α* marked decrease in the *α* value. Sintering at 1300 °C resulted in excessively large grains (10.42 μm), which may indicate aberrant grain development mechanism. This microstructural condition induced inhomogeneous spatial distribution of DSBs throughout the ceramic matrix. Electrical properties deteriorated as a direct result of the consequent shortage of electroactive barrier sites, with a substantial decline in both the breakdown voltage and the nonlinearity coefficient. This trend, illustrated in Figure 9, suggests that the varistor achieves optimal performance characteristics at a firing temperature of 1250 °C. Processing at 1250 °C established the optimal sintering regime for this system, achieving the confluence of favorable microstructural and electrical properties. The sample demonstrated outstanding densification (relative density >96%), with complete suppression of porosity. Microstructural uniformity was evidenced by sharp, well-resolved XRD diffraction peaks. These superior microstructural characteristics enabled maximum grain boundary barrier formation, as evidenced by the highest nonlinearity coefficient (α = 3.85) and a stable barrier height (0.66 eV), establishing that this sintering temperature optimally balances grain growth with double Schottky barrier stability and effectiveness. It also supports the notion that lower sintering temperatures may lead to the formation of ceramics with a weakly nonlinear response, as they are insufficient to produce highly effective grains. The observed reduction in E_B with rising sintering temperature is due to the diminished number of grain boundaries caused by the enlarged ZnO grain size and a reduction in the varistor V_{gb} [11]. Since E_B arises from voltage surges across each grain boundary, a decrease in active barriers within the microstructure results in variations within a lower electric field [20]. As the sintering temperature increases, the breakdown voltage per grain boundary slightly diminishes from 0.2 to 0.1 V. Conversely, a higher φ_B is associated with an increased *α* value in relation to the sintering temperature, achieving optimal nonlinear electrical characteristics at 1250 °C.

A possibly small value of leakage current density, J_L is one of the ideal properties in a varistor to avert the device from the thermal runaway generated by high leakage current as the heat is not relocated to the outside surroundings. The decreased in J_L is attributed to the high grain boundary barriers, which restrict charge transport transition [4]. With an increase in sintering temperature from 1100 °C to 1250 °C, the leakage current density experiences a marked reduction. However, upon further increasing the sintering temperature to 1300 °C, the leakage current density rises once more. This measured leakage current is inversely proportional to the barrier height, with values ranging from 746 to 425 μA/cm² and barrier heights between 0.60 and 0.67 eV, respectively. Further increases in the sintering temperature of the varistor beyond 1250 °C resulted in notable microstructural changes. Specifically, sintering at temperatures above this threshold led to an uneven or inhomogeneous distribution of DSBs within the grain boundaries. The formation of larger ZnO grains at elevated temperatures reduces the number of effective grain boundaries per unit thickness of the varistor material. The crucial structural element that permits barrier formation is oxygen vacancies and the defect states that accompany them, in which lack of them would abolish the varistor nonlinearity and result in the material

exhibiting the ohmic behavior typical of simple resistors [16]. Consequently, this decrease in grain boundary density diminishes the likelihood of nonlinear electrical conductivity occurring across the double Schottky barriers present at these boundaries. Through two complimentary mechanisms, the TiO_2 phase found in the $CaTiO_3$ dopant system enhances varistor performance. Microstructurally, TiO_2 promotes the diffusion and coalescence of zinc and oxygen species during sintering by lowering the activation energy for ion migration, which enhances solid-state grain development. Electrically, the oxygen-rich composition of the intergranular titanate phase enhances potential barrier formation at grain boundaries. The elevated oxygen content strengthens the electrostatic barrier structure, thereby amplifying the material's voltage-clamping capability for effective suppression of voltage transients [47].

4.0 CONCLUSION

This study systematically investigated the effect of sintering temperature (1100 to 1300 °C) on the microstructure and electrical properties of ZnO-$CaTiO_3$ composite varistor ceramics. The findings demonstrate that sintering temperature is a critical parameter governing varistor performance. Increasing sintering temperature from 1100 to 1300 °C promoted progressive ZnO grain growth (4.66 to 10.42 µm) and enhanced densification (relative density >94%). The XRD analysis revealed that the spinel phase (Zn_2TiO_4) formed at lower temperatures (1100 to 1200 °C) but dissolved or was suppressed above 1200 °C. Crystal quality improved at higher temperatures, as evidenced by sharper XRD peaks and increased crystallite size (34.46 to 60.15 nm). The nonlinearity coefficient (α) increased with sintering temperature, reaching a maximum of 3.85 at 1250 °C, accompanied by an optimal barrier height of 0.66 eV and minimal leakage current density of 425 µA/cm². However, further temperature increased to 1300 °C caused α to drop sharply, correlating with excessive grain growth and reduced grain boundary density. The 1250 °C sintering condition represents the optimal sintering temperature in achieving complete densification (relative density >96%), uniform microstructure, and superior electrical properties with breakdown voltage of 0.99 V/mm. At 1300 °C, excessive grain coarsening (10.42 µm) and degraded grain boundary barriers resulted in diminished electrical performance. The research confirms that TiO_2 (from $CaTiO_3$) effectively promotes grain growth and densification while enhancing barrier formation through oxygen enrichment at grain boundaries. These findings provide fundamental guidance for optimizing sintering parameters in the design of low-voltage ZnO-based varistors with ideal nonlinear electrical characteristics and enhanced surge protection capability.

Acknowledgement

This work was supported by the Ministry of Higher Education Malaysia and Universiti Malaysia Terengganu under the research project through the Talent and Publication Enhancement-Research Grant (TAPE-RG/2022/Vot. No. 55385).

Conflicts of Interest

The authors declare that there is no conflict of interest regarding the publication of this paper.

References

[1] Drabkin, M. 2002. Surge Protection of Low-Voltage AC Power by MOV-Based SPDs. In *Proceedings of the 10th International Conference on Harmonics and Quality of Power*. IEEE.
[2] Boumezoued, A., *et al*. 2019. ZnO Nanopowders Doped with Bismuth Oxide: From Synthesis to Electrical Application. *Journal of Alloys and Compounds*. 791: 550–58.
[3] Topcagic, Z., and T. E. Tsovilis. 2021. Varistor Electrical Properties: Microstructural Effects. In *Encyclopedia of Materials: Technical Ceramics and Glasses*. 254–71.
[4] Li, J., *et al.* 2021. Effects of Pre-Calcination and Sintering Temperature on the Microstructure and Electrical Properties of ZnO-Based Varistor Ceramics. *Materials Science in Semiconductor Processing*. 123.
[5] Leach, C., Z. Ling, and R. Freer. 2000. The Effect of Sintering Temperature Variations on the Development of Electrically Active Interfaces in Zinc Oxide-Based Varistors. *Journal of the European Ceramic Society*. 20(16): 2759–65.
[6] Borysiewicz, M. A. 2019. ZnO as a Functional Material: A Review. *Crystals*. 9(10).
[7] Xie, P., and J. Hu. 2019. Influence of Sintering Temperature and ZrO_2 Dopants on the Microstructure and Electrical Properties of Zinc Oxide Varistors. *IEEE Access*. 7: 140126–33.
[8] Hewlett, R. M., and M. A. McLachlan. 2016. Surface Structure Modification of ZnO and the Impact on Electronic Properties. *Advanced Materials*. 28(20): 3893–3921.
[9] Chen, T., *et al.* 2016. Novel Synthesis of Monodisperse ZnO-Based Core/Shell Ceramic Powders and Applications in Low-Voltage Varistors. *Materials & Design*. 96: 329–34.
[10] Ghazali, M. S. M., *et al*. 2016. The Sintering Effect of Lanthanum-Calcium Manganite Doping on Microstructure and Non-Linear Coefficient of Zinc Oxide Varistor. *Materials Science Forum*. 846: 142–48.
[11] Chen, G.-H., *et al.* 2015. Sintering Temperature Dependence of Varistor Properties and Impedance Spectroscopy Behavior in ZnO-Based Varistor Ceramics. *Journal of Materials Science: Materials in Electronics*. 26(4): 2389–96.
[12] Ahmed, Z. W., A. I. Khadim, and A. H. R. Alsarraf. 2019. The Effect of Doping with Some Rare Earth Oxides on Electrical Features of ZnO Varistor. *Energy Procedia*. 157: 909–17.
[13] Desouky, O. A., and K. E. Rady. 2016. Improvement of Sintering, Nonlinear Electrical, and Dielectric Properties of ZnO-Based Varistors Doped with TiO_2. *Chinese Physics B*. 25(6).
[14] de Salles, C., *et al.* 2016. Effects of Operation Temperature in Artificially Aging of Zinc Oxide Varistors by High-Current Short Impulses. *Electric Power Systems Research*. 134: 145–51.

[15] Bai, H., *et al*. 2016. Influence of Cr_2O_3 on Highly Nonlinear Properties and Low Leakage Current of ZnO–Bi_2O_3 Varistor Ceramics. *Ceramics International.* 42(9): 10547–50.
[16] Xie, P., Z. Wang, and K. Wu. 2022. Evolution of Intrinsic and Extrinsic Electron Traps at Grain Boundary during Sintering ZnO-Based Varistor Ceramics. *Materials* .15(3).
[17] Zhao, X., *et al.* 2018. Introducing a ZnO–PTFE (Polymer) Nanocomposite Varistor via the Cold Sintering Process. *Advanced Engineering Materials.* 20(7).
[18] Mahesh, K., *et al.* 2013. Effect of Two-Step Sintering on Rare Earth (RE = Y_2O_3, Pr_6O_{11})-Doped ZnO–Bi_2O_3 Varistors Processed from 'Nano-Precursor' Powders. *Journal of Materials Science: Materials in Electronics.* 24(5): 1495–1504.
[19] Ghazali, M. S. M., *et al*. 2018. Conventional Sintering Effects on the Microstructure and Electrical Characteristics of Low-Voltage Ceramic Varistor. In *Sintering Technology—Method and Application*.
[20] Badruddin, M. A., *et al.* 2022. Electrical and Microstructural Evaluation of ZnO Varistor Ceramics with Different $CaSiO_3$ Contents. *Materials Chemistry and Physics.* 289.
[21] Zahid, R. 2011. Effect of Temperature Treatment on the Optical Characterization of ZnO–Bi_2O_3–TiO_2 Varistor Ceramics. *International Journal of Physical Sciences.* 6(6): 1388–94.
[22] Shahraki, M. M., M. A. Bahrevar, and S. M. S. Mirghafourian. 2015. The Effect of TiO_2 Addition on Microstructure and Electrical Properties of SnO_2 Varistors Prepared from Nanomaterials." *Ceramics International.* 41(5): 6920–24.
[23] Tairi, L., *et al*. 2022. Enhanced Photoluminescence and Photocatalytic Activity of Ca^{2+} Addition into ZnS Nanoparticles Synthesized by Hydrothermal Method. *Physica B: Condensed Matter.* 631: 413713.
[24] Lungu, M. V. 2023. Effects of Dopants and Processing Parameters on the Properties of ZnO–V_2O_5-Based Varistors Prepared by Powder Metallurgy: A Review. *Materials.* 16(10): 3725.
[25] Wurst, J. 1972. Linear Intercept Technique for Measuring Grain Size in Two-Phase Polycrystalline Ceramics. *Journal of the American Ceramic Society.* 55: 109.
[26] Mendelson, M. I. 1969. Average Grain Size in Polycrystalline Ceramics. *Journal of the American Ceramic Society*. 52(8): 443–46.
[27] Anas, S., *et al.* 2017. Sol-Gel Materials for Varistor Devices. In *Sol-Gel Materials for Energy, Environment and Electronic Applications*. 23–59. Springer.
[28] Wong, J. 1980. Sintering and Varistor Characteristics of ZnO–Bi_2O_3 Ceramics. *Journal of Applied Physics.* 51(8): 4453–59.
[29] Mirzayi, M. 2020. The Effect of TiO_2 Concentration on the Electrical and Microstructural Properties of ZnO-Based Varistor Ceramic Prepared from Nanosize ZnO Particles. *Advances in Applied Ceramics.* 119(7): 373–79.
[30] Bouchekhlal, A., and M. Boulesbaa. 2022. Synthesis and Characterization of ZnO-Based Varistor Ceramics: Effect of Sintering Temperatures. *Microelectronics International.* 39(3): 110–20.
[31] Richardson, J. J., *et al.* 2011. Thermally Induced Pore Formation in Epitaxial ZnO Films Grown from Low-Temperature Aqueous Solution. *Crystal Growth & Design.* 11(8): 3558–63.
[32] Hembram, K., *et al.* 2021. CaO-Doped ZnO–Bi_2O_3 Varistors: Grain Growth Mechanism, Structure, and Electrical Properties. *Ceramics International.* 47(1): 1229–37.
[33] Zhang, Y., *et al.* 2017. Spinel and Post-Spinel Phase Assemblages in Zn_2TiO_4: An Experimental and Theoretical Study. *Physics and Chemistry of Minerals.* 44(2): 109–23.
[34] Syaizwadi, S. M., *et a*l. 2021. Nonlinearity Characteristics of Low-Voltage Barium Titanate-Based Zinc Oxide Varistor Ceramics Modified by Cobalt Dopants. *Journal of Integrated Circuits and Systems.* 16(1): 1–7.
[35] Janani, F. Z., *et al.* 2022. ZnO–Zn_2TiO_4 Heterostructure for Highly Efficient Photocatalytic Degradation of Pharmaceuticals. *Environmental Science and Pollution Research*. 1–14.
[36] Syaizwadi, S. M., *et al.* 2018. Effect of Sintering Temperature on Zinc Oxide Varistor Ceramics. In *IOP Conference Series: Materials Science and Engineering*. IOP Publishing.
[37] Wang, C.-L., *et al*. 2014. Phase Formation of Zinc Titanate Precursor Prepared by a Hydrothermal Route at pH 5. *Ceramics International.* 40(5): 7407–15.
[38] Lokesh, B., S. Kaleemulla, and N. M. Rao. 2014. Synthesis and Characterization of Zinc Titanates by Solid-State Reaction. *International Journal of ChemTech Research.* 6: 1929–32.
[39] Sangeetha, A., *et al*. 2019. Correlation between Calcination Temperature and Optical Parameter of Zinc Oxide (ZnO) Nanoparticles. *Journal of Sol-Gel Science and Technology*. 91: 261–72.
[40] Upadhyay, S., K. Parekh, and B. Pandey. 2016. Influence of Crystallite Size on the Magnetic Properties of Fe_3O_4 Nanoparticles. *Journal of Alloys and Compounds.* 678: 478–85.
[41] Park, J. H., *et al.* 2015. Analysis of Oxygen Vacancy in Co-Doped ZnO Using the Electron Density Distribution Obtained Using MEM. *Nanoscale Research Letters.* 10(1): 186.
[42] Cui, F., *et al.* 2021. Low-Temperature Sintering ZnO–Bi_2O_3-Based Varistor Ceramics with Low Electrical Breakdown Voltage and High Nonlinear Coefficient. *Ceramics International.* 47(3): 4118–26.
[43] Shaifudin, M. S., *et al*. 2021. Synergistic Effects of Pr_6O_{11} and Co_3O_4 on Electrical and Microstructure Features of ZnO–$BaTiO_3$ Varistor Ceramics. *Materials.* 14(4).
[44] Akinnifesi, J. O., and O. O. Akinwunmi. 2015. Effect of Sintering Temperature on the Microstructure and Electrical Characteristics of Low-Clamping-Voltage Zinc Oxide-Based Ceramic Varistor. *Journal of Materials Science Research.* 4(3): 40–48.
[45] Meng, P., *et a*l. 2024. Breakdown Mechanism Induced by Edge Pore Defects in ZnO Varistors and Improvement of Energy Capacity by Applying an In Situ Repair Medium. *Journal of the European Ceramic Society*. 44(6): 3877–86.
[46] Hembram, K., *et al*. 2020. Influence of CaO Doping on Phase, Microstructure, Electrical, and Dielectric Properties of ZnO Varistors. *Journal of Alloys and Compounds* 817.
[47] Tian, T., *et al*. 2024. Influence of TiO_2 Doping on the Grain Growth and Electrical Properties of ZnO–Cr_2O_3-Based Varistor Ceramics. *Journal of Alloys and Compounds.* 1008: 176657.